Supporting Information

Guo et al. 10.1073/pnas.1215563110

SI Text S1: Methods

Sample Preparation. The bacteriophage T7 capsid I sample was prepared according to established procedures (1). Briefly, 6 L of *Escherichia coli* BB/1 was grown to 4×10^8 per mL and inoculated with T7 amber mutant in genes 5 (DNA polymerase) and 19 (packaging ATPase) at a multiplicity of 4. Packaging does not occur, but accumulation of capsid I does, even though phage DNA is not replicated. Lysis was completed by adding chloroform. The capsid I particles were precipitated with polyethylene glycol and resuspended. The resuspended particles were clarified by low-speed centrifugation and DNase digested. The capsid I particles were purified by two CsCl gradient centrifugations, first through a step gradient and then within a buoyant density gradient. Particles of the capsid I band were collected and then dialyzed into 0.2 M NaCl, 0.01 M Tris·Cl, pH 7.4, and 0.001 M $MgCl_2$. The primary contaminant was an occasional outer membrane vesicle that was almost always smaller than capsid I (1).

Electron Cryomicroscopy. A 3-μL aliquot of T7 capsid I sample was applied to a 400 mesh lacey carbon grid with a thin layer of continuous carbon film (Ted Pella). After blotting away the excessive sample solution, the grid was plunged-frozen at liquid N_2 temperature using the FEI Vitrobot. A FEI Titan Krios 300-kV electron cryomicroscope was used to image the samples using low-dose (~25 e/Å^2) imaging technique at liquid N_2 temperature. A total of 1,270 images was taken at 59,000 nominal magnification and recorded on Kodak 163 negative films with targeted underfocus range of 1–4 μm. The films were scanned using a Nikon SuperCoolScan 9000 scanner. The final calibrated sampling of the scanned images is 1.1 Å/pixel. The magnifications were calibrated using the MAG*I*CAL grid (EM Sciences), imaged, and scanned at identical conditions.

Image Processing and 3D Reconstruction. T7 capsid I particles (~30,000 in total) were selected from scanned micrograph images, first automatically by the *ethan* method (2) and then by manual screening with the EMAN (3) *boxer* program. The transmission electron microscope instrument contrast transfer function parameters were determined automatically using *fitctf2.py* (4, 5) and then visually validated using EMAN *ctfit* program. For 3D reconstructions, the images were first binned 4× to make initial reconstructions. After the alignment parameters and reconstructions converged, the 2× binned images were used for final reconstructions with a sampling of 2.2 Å/pixel.

Icosahedral reconstruction. The particles were first reconstructed as icosahedral particles with initial model built from randomly assigned initial orientations and iterative refinements of the orientations. Consistent icosahedral capsid structures (other than occasional difference in handedness) were obtained by repeating the random model process. After elimination of particles of inconsistent view parameters, about 10,000 particles were included in further image processing and reconstructions.

Standard asymmetric reconstruction. The orientation of every particle from the icosahedral reconstruction, which was limited to a single icosahedral asymmetric unit (1/60 of entire rotational space), was then randomly reassigned to 1 of the 60 icosahedral symmetry-related views. These newly assigned views were used to build the initial asymmetric model (i.e., no symmetry enforced). Note that the initial asymmetry reconstruction model was built completely from the particles without any assumptions on the location, size, or shape of the nonicosahedral components. This is in contrast with earlier asymmetric reconstructions that used explicit asymmetric features to bootstrap the iterative refinements (6, 7). An iterative symmetric relaxation (icosahedral symmetry to c1 symmetry) alignment similar to our earlier approach (6, 7) was then used to obtain converged asymmetric reconstructions. To ensure that correct asymmetric reconstruction was obtained, the above process of building random initial asymmetric model and iterative symmetric relaxation alignment was repeated multiple times to obtain consistent asymmetric structures (other than occasional difference in the location, $+Z$ or $-Z$ axes, where the portal/core showed up).

Focused asymmetric reconstructions. The above standard asymmetric reconstruction (SAR) reconstruction was obtained using all structural components in the alignment (red circle in Fig. S4). Focused asymmetric reconstructions (FARs) were then obtained with alignment using only a subset of the structural components. The corresponding symmetry relaxations were the following: c5→c1 for portal from shell orientation, c12→c1 for core from portal orientation, c8→c1 for portal from core, and c8→c1 for core tip region from core main body, etc. The red circles in Figs. S5–S7 (Table S1) indicate the regions of focus for FAR reconstruction of the different combinations of the five structural components [icosahedral shell gene product 10 (gp10), 12-fold portal gp8, 12-fold gp14, 8-fold gp15, and 4-fold gp16] (Table S1). The focused alignment was done by soft masking the corresponding structure region in the asymmetry 3D reconstructions so that only this region is included in projections (red circles in Figs. S5–S7). The masks were all spherical masks centered at different Z positions on the portal vertex axis (i.e., the icosahedral fivefold axis). The same 3D mask is projected to generate a 2D soft mask to only include the corresponding region of the 2D particle images for alignment. In other work, similar masking was used in a focused classification method for solving structures of heterogeneous protein complexes with or without bound ligands (8). Note that no symmetry was imposed in any of the asymmetric reconstructions. Either resolved or smeared structure in the reconstructions is due to the intrinsic structural features, including the consistency of features among different particles.

All of the above icosahedral and asymmetric reconstructions were performed with in-house developed programs, *jspr.py* (for overall workflow), *jalign* (for 2D alignment), and *j3dr* (for 3D reconstruction) that use EMAN (3) and EMAN2 (9) library functions. These programs will be made available from the author's Web site (http://jiang.bio.purdue.edu). The resolutions of the reconstructions were evaluated by Fourier shell correlation (10) (0.5 criterion) of the two reconstructions built from complementary halves of the datasets (Fig. S10). The eight reconstructions (Icos, SAR, and FAR-I to FAR-VI) were deposited to Electron Microscopy Databank with accession numbers (EMD-5566–EMD-5573).

Structural Analysis. The 2D section views were displayed using EMAN *eman* program and IMOD (11) *3dmod* program. The EMAN *qsegment* and the Chimera (12) programs were used to segment each of the structural components in the whole reconstruction maps. The 3D maps were displayed using Chimera program. The symmetry axis analysis (Fig. 4*A* and Fig. S11) was performed using the in-house developed *refineSymmetryAxis.py* program that searches best axis position and direction to maximize the rotational symmetry quality (13).

SI Text S2: Why is Eightfold gp15 Resolved in SAR?

In SAR reconstruction, the well-resolved fivefold shell and eightfold gp15 layer of the core stack are separated by the rotationally smeared gp8 portal and gp14 core stack layer (Figs. 1 and 2, and Figs. S3 and S4). This surprising arrangement of resolved features in SAR was the major driving force for the development of FAR procedure. We used the FAR reconstructions to find that the five layers (5-fold shell, 12-fold gp8 portal and gp14 layer, 8-fold gp15 layer, and 4-fold gp16 layer) of the portal vertex are arranged in tandem with uncorrelated symmetry mismatches. The variability of relative axial rotation occurred at all of the symmetry-mismatched layer interfaces. Therefore, in principle, layers separated by one (or more) intermediate layer of different symmetry should not be simultaneously resolved. Although the FAR reconstructions confirm this conclusion (FAR-I to FAR-VI, summarized in Table S1), the SAR reconstruction does not, which necessitates an explanation.

To find an explanation, we analyzed the relative layer orientations for all possible combinations of symmetry mismatches generated by both 5–12–8 symmetries (seen via FAR-I to FAR-II) and 5–8 symmetries (seen via SAR) (Dataset S1). We found that, for every 5-, 12-, 8-fold combination of orientations, a 5-, 8-fold combination could be found that resulted in either zero (Fig. S12*A*, one-third of all combinations) or a small angular error (3°) (Fig. S12*B*, two-thirds of all combinations) for the relative view of the 5- and 8-fold layers. Therefore, it is likely that the reinforcement of the eightfold gp15 layer during SAR is the result of approximate aligning a single 5-, 8-fold combination to multiple particles of different 5–12–8 combinations, with varying orientation of intermediate 12-fold layer. For example, two combinations are shown in Fig. S12. If so, the well-resolved fivefold gp10 shell and eightfold gp15 layer sandwiching the smeared gp8 portal/gp14 layer in the SAR reconstruction was due to the dominance of the gp10 shell and gp15 core stack features (5–8 combination) in alignments for T7 capsid I particles. We note that the statistical aspect of the gp15 layer reinforcement suggests the possibility of occasional errors in the symmetry found via SAR. Although the SAR-derived symmetry for the T7 gp15 layer was correct, the use of FAR is essential to validate the symmetries.

More detailed illustrations of above explanation are shown in Fig. S12. In Fig. S12*A*, the marked vertex of the intermediate 12-fold ring is perfectly aligned with the marked vertices of the 5-fold and 8-fold rings. In contrast, if one aligns the 8-fold ring with the next vertex of the 12-fold ring, the best aligned 5-fold vertex (F1) and 8-fold vertex (E1) are offset by 3° and the intermediate 12-fold ring is close to the midpoint of its two neighbor vertices (Fig. S12*B*). In SAR reconstruction of T7 capsid I, due to the more dominant 8-fold g15 layer over the 12-fold gp8 and gp14 layer in alignment, particles with these two different 5–12–8 combinations were averaged with their 5-fold vertices (marked in Fig. S12*A* and F1 in Fig. S12*B*) aligned and the 8-fold vertices (marked in Fig. S12*A* and E1 in Fig. S12*B*) approximately aligned with 3° error. However, the intermediate 12-fold ring was averaged with its vertex (marked in Fig. S12*A*) aligned to a position near the midpoint of its two neighboring vertices (Fig. S12*B*), which led to rotational smearing of the 12-fold ring, as observed in our SAR reconstruction.

The FAR-IV and FAR-V reconstructions (Fig. S8) used the 8-fold gp15 layer from SAR as starting points to sequentially resolve the 12-fold gp8 portal/gp14 core stack layer and the 5-fold gp10 shell, respectively. Similar to the results of FAR-I and FAR-II, the 8-fold gp15 core stack layer and 12-fold gp14/gp8 layer became resolved in FAR-IV, and the 12-fold gp8/gp14 layer and 5-fold shell became resolved in FAR-V reconstructions. However, both the portal and the shell were slightly less resolved than in FAR-II and FAR-I, suggesting that the small initial angular errors (3°) for gp15 in the starting SAR reconstruction have propagated to the subsequent reconstructions (FAR-IV and FAR-V).

SI Text S3: FAR Reconstructions Represent a Special Case of a Paradigm in Structural Biology: Combinatorial Assembly Isomerism

In *Discussion*, *A Paradigm in Structural Biology: Combinatorial Assembly Isomerism*, we presented the idea that the FAR reconstructions in this study represent a special case of a more general regime of structural biology: combinatory assembly isomerism. Here, we will further elaborate on this point. An analogy for this regime is use of a single set of LEGO pieces to assemble different objects. A more technical description of this regime is that N (n = the number of structural components, $n > 1$) sets of orientation and position parameters $(a_i, \beta_i, \gamma_i, x_i, y_i; i = 1, 2, \ldots, N)$ (Fig. S13*B*) are needed to describe a particle image, whereas a single set of orientation and position parameters $(\alpha, \beta, \gamma, x, y)$ (Fig. S13*A*) is sufficient to describe a nonisomeric particle assumed for past asymmetric reconstructions. The FAR reconstructions deal with a special case of this regime in which last two of the three orientation parameters (Euler angles) are constrained to similar values and the first orientation parameters are related by $\alpha_{j+1} - \alpha_j = i\frac{2\pi}{M_j}$ $(i \in [0, M_j - 1]$ and M_j is the rotational symmetry of component $j)$ for two adjacent layers.

We note that the combinatorial assembly isomerism discussed here is different from the heterogeneity that has received much attention in recent years (14, 15). This heterogeneity is characterized by only a small number of discrete states. Particles are first classified into subgroups, and, within each group, particles are assumed to have identical structure. In contrast, the combinatorial assembly isomerism can involve very large number of different states due to exponential increase in the number of combinations. The isomerism addressed here is thus more analogous to extreme heterogeneity in which the conformations can vary continuously and no two particles have the same structure.

1. Fang PA, et al. (2008) Visualization of bacteriophage T3 capsids with DNA incompletely packaged in vivo. *J Mol Biol* 384(5):1384–1399.
2. Kivioja T, Ravantti J, Verkhovsky A, Ukkonen E, Bamford D (2000) Local average intensity-based method for identifying spherical particles in electron micrographs. *J Struct Biol* 131(2):126–134.
3. Ludtke SJ, Baldwin PR, Chiu W (1999) EMAN: Semiautomated software for high-resolution single-particle reconstructions. *J Struct Biol* 128(1):82–97.
4. Yang C, et al. (2009) Estimating contrast transfer function and associated parameters by constrained non-linear optimization. *J Microsc* 233(3):391–403.
5. Jiang W, Guo F, Liu Z (2012) A graph theory method for determination of cryo-EM image focuses. *J Struct Biol* 180(2):343–351.
6. Chang J, Weigele P, King J, Chiu W, Jiang W (2006) Cryo-EM asymmetric reconstruction of bacteriophage P22 reveals organization of its DNA packaging and infecting machinery. *Structure* 14(6):1073–1082.
7. Jiang W, et al. (2006) Structure of epsilon15 bacteriophage reveals genome organization and DNA packaging/injection apparatus. *Nature* 439(7076):612–616.
8. Penczek PA, Frank J, Spahn CM (2006) A method of focused classification, based on the bootstrap 3D variance analysis, and its application to EF-G-dependent translocation. *J Struct Biol* 154(2):184–194.
9. Tang G, et al. (2007) EMAN2: An extensible image processing suite for electron microscopy. *J Struct Biol* 157(1):38–46.
10. Harauz G, Vanheel M (1986) Exact filters for general geometry 3-dimensional reconstruction. *Optik (Stuttg)* 73(4):146–156.
11. Kremer JR, Mastronarde DN, McIntosh JR (1996) Computer visualization of three-dimensional image data using IMOD. *J Struct Biol* 116(1):71–76.
12. Goddard TD, Huang CC, Ferrin TE (2007) Visualizing density maps with UCSF Chimera. *J Struct Biol* 157(1):281–287.
13. He J, Schmid MF, Zhou ZH, Rixon F, Chiu W (2001) Finding and using local symmetry in identifying lower domain movements in hexon subunits of the herpes simplex virus type 1 B capsid. *J Mol Biol* 309(4):903–914.
14. Leschziner AE, Nogales E (2007) Visualizing flexibility at molecular resolution: Analysis of heterogeneity in single-particle electron microscopy reconstructions. *Annu Rev Biophys Biomol Struct* 36:43–62.
15. Scheres SH (2010) Classification of structural heterogeneity by maximum-likelihood methods. *Methods Enzymol* 482:295–320.

Reconstructions	Note
EMD-1163	T7 phage state "C1" reconstruction *(http://www.ebi.ac.uk/pdbe-srv/emsearch/atlas/1163_summary.html)*
EMD-1164	T7 phage state C5 reconstruction *(http://www.ebi.ac.uk/pdbe-srv/emsearch/atlas/1164_summary.html)*
EMD-1715	P-SSP7 phage state C1 reconstruction *(http://www.ebi.ac.uk/pdbe-srv/emsearch/atlas/1715_summary.html)*
EMD-1175	Epsilon15 phage state C1 reconstruction *(http://www.ebi.ac.uk/pdbe-srv/emsearch/atlas/1175_summary.html)*

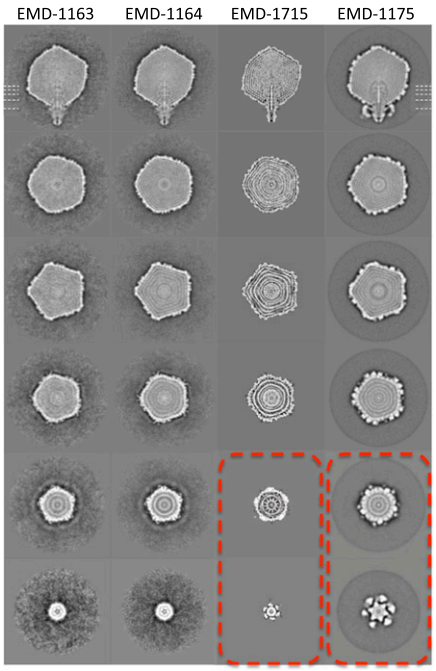

Fig. S1. Comparison of previously reported asymmetric reconstructions of dsDNA bacteriophages with internal structures resembling the T7 core stack. Structures EMD-1163 for T7 phage (asymmetric) (1), EMD-1164 for T7 phage (fivefold averaging) (1), EMD-1715 for P-SSP7 phage (asymmetric) (2), and EMD-1175 for ε15 phage (asymmetric) (3) were adjusted to same view and scale for comparison. The background region was already masked in the deposited P-SSP7 phage structure. A central section parallel to the portal/core stack axis is shown in the top row. The subsequent rows display the five sections (indicated by dashed lines in the top row) perpendicular to this portal/core stack axis. The 12-fold portal and the 6-fold tail hub regions in these asymmetric reconstructions were only resolved in the structure of P-SSP7 and ε15 phage (dashed red boxes), but not in the two structures of T7 phage. The rotational symmetry of the core stack proteins (rows 2–4) was not resolved in any of these four structures.

1. Agirrezabala X, et al. (2005) Maturation of phage T7 involves structural modification of both shell and inner core components. *EMBO J* 24(21):3820–3829.
2. Liu X, et al. (2010) Structural changes in a marine podovirus associated with release of its genome into Prochlorococcus. *Nat Struct Mol Biol* 17(7):830–836.
3. Jiang W, et al. (2006) Structure of epsilon15 bacteriophage reveals genome organization and DNA packaging/injection apparatus. *Nature* 439(7076):612–616.

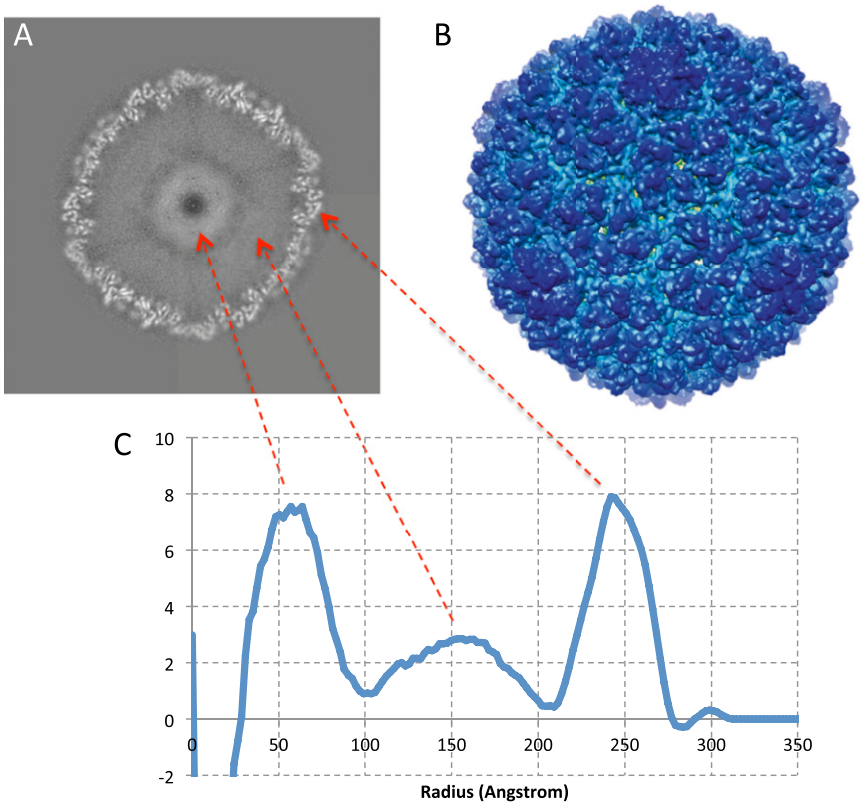

Fig. S2. Icosahedral reconstruction of T7 capsid I. (*A*) Raw density image in central section, viewed along a twofold axis. (*B*) Radially colored surface view along a threefold axis. (*C*) Rotationally averaged radial density distribution. The arrows indicate the source in *A* of the density peaks in the curve of *C*.

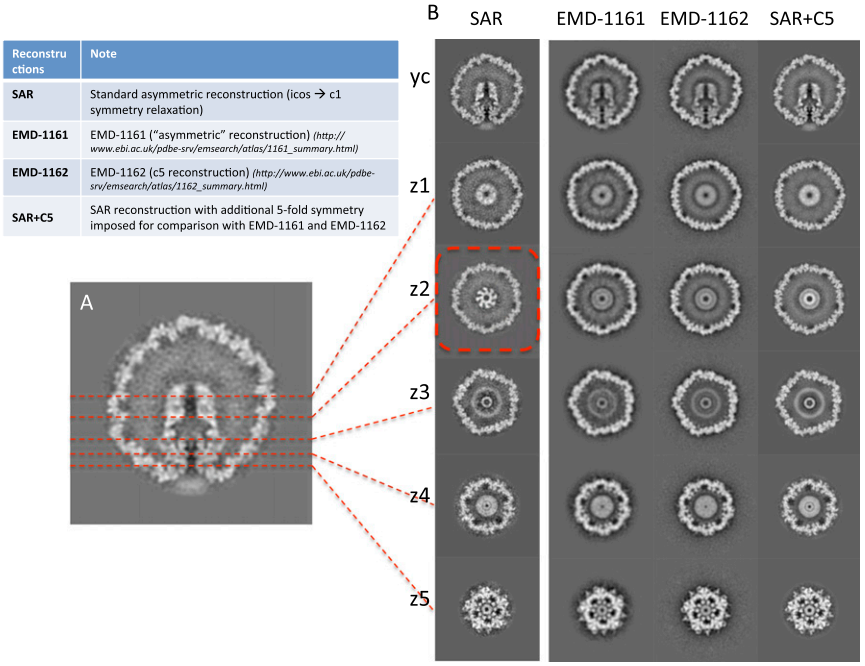

Reconstructions	Note
SAR	Standard asymmetric reconstruction (icos → c1 symmetry relaxation)
EMD-1161	EMD-1161 ("asymmetric" reconstruction) *(http://www.ebi.ac.uk/pdbe-srv/emsearch/atlas/1161_summary.html)*
EMD-1162	EMD-1162 (c5 reconstruction) *(http://www.ebi.ac.uk/pdbe-srv/emsearch/atlas/1162_summary.html)*
SAR+C5	SAR reconstruction with additional 5-fold symmetry imposed for comparison with EMD-1161 and EMD-1162

Fig. S3. Comparison of standard asymmetric reconstructions of T7 capsid I. (*A*) Central section of SAR cut parallel to the portal/core stack axis. (*B*, *Left*) SAR-derived sections cut perpendicular to the portal/core stack axis at the five axial locations indicated by the dashed lines in *A*. The red box indicates the section with resolved eightfold gp15 features. (*B*, *Right*) The same set of sections for the two T7 capsid I reconstructions (EMD-1161: asymmetric reconstruction; EMD-1162: fivefold symmetric reconstruction) reported in ref. 1, and our SAR reconstruction with additional fivefold symmetry imposed (SAR+C5). The eightfold symmetric structural features were only resolved in our SAR, but not in EMD-1161, EMD-1162, and SAR+C5. The rotational symmetry of other proteins in the portal complex (gp8 portal, gp14 and gp16 core stack layers) was not resolved in any of these four structures.

1. Agirrezabala X, et al. (2005) Maturation of phage T7 involves structural modification of both shell and inner core components. *EMBO J* 24(21):3820–3829.

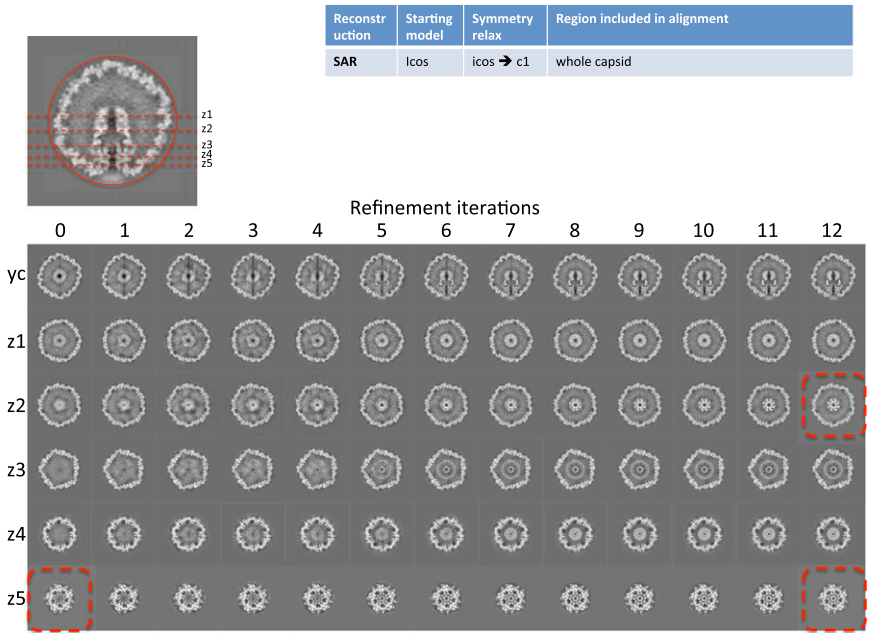

Fig. S4. Refinement convergence for standard asymmetric reconstruction (SAR). Only the first 12 iterations are shown. The numbers at the top (0–12) indicate the refinement iterations with 0 referring to the starting icosahedral model. The first row (yc) shows the central section cut parallel to the portal/core stack axis. The subsequent rows (z1, z2, z3, z4, z5) show different sections cut perpendicular to the portal/core stack axis, as indicated in Fig. 1*C*. The entire particle, as indicated by the red circle, was included in the alignment. The dashed red boxes indicate the sections with resolved features of the portal vertex.

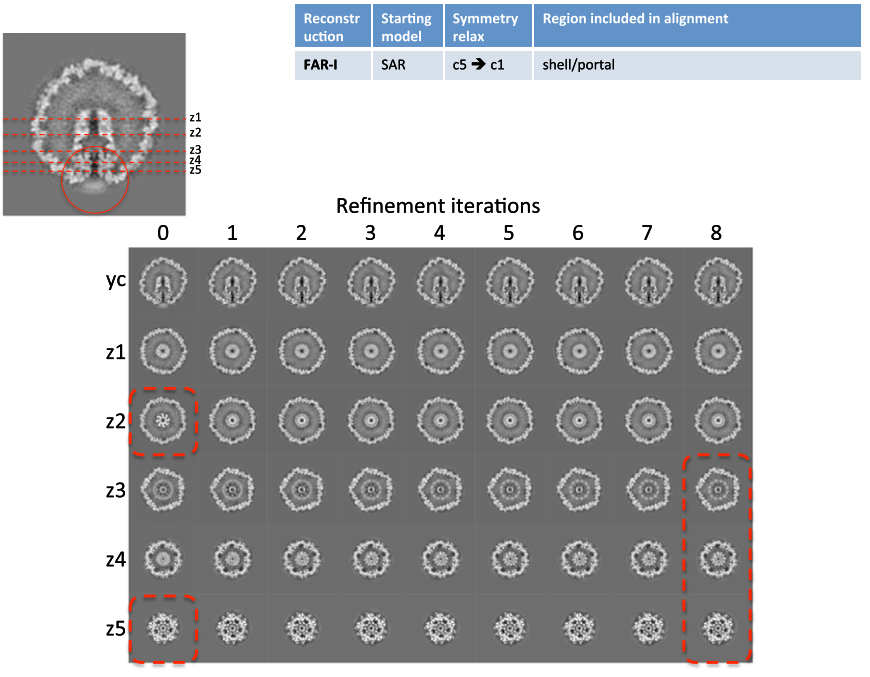

Fig. S5. Refinement convergence for focused asymmetric reconstruction I (FAR-I). Only the first eight iterations are shown. The numbers on the top (0–8) indicate the refinement iterations with 0 referring to the starting model (SAR). The first row (yc) shows the central section cut parallel to the portal/core stack axis. The subsequent rows (z1, z2, z3, z4, z5) show different sections cut perpendicular to the portal/core stack axis, as indicated in Fig. 1*C*. The red circle in the upper left corner indicates the region included in the alignment. The dashed red boxes indicate the sections with resolved features of the portal vertex.

Reconstruction	Starting model	Symmetry relax	Region included in alignment
FAR-II	FAR-I	c12 → c1	portal/core

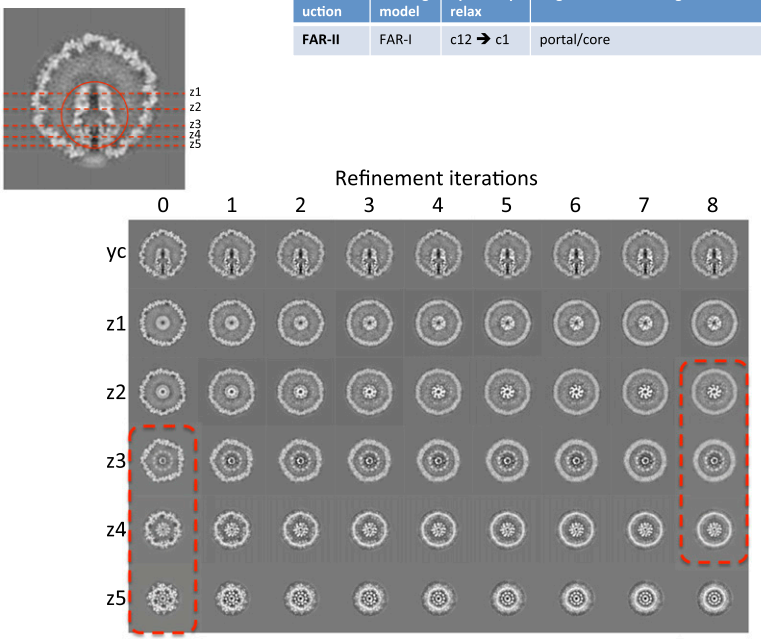

Fig. S6. Refinement convergence for focused asymmetric reconstruction II (FAR-II). Only the first eight iterations are shown. The numbers at the top (0–8) indicate the refinement iterations with 0 referring to the starting model (FAR-I). The first row (yc) shows the central section cut parallel to the portal/core stack axis. The subsequent rows (z1, z2, z3, z4, z5) show different sections cut perpendicular to the portal/core stack axis, as indicated in Fig. 1*C*. The red circle in the upper left corner indicates the region included in the alignment. The dashed red boxes indicate the sections with resolved features of the portal vertex.

Reconstruction	Starting model	Symmetry relax	Region included in alignment
FAR-III	FAR-II	c8 → c1	core

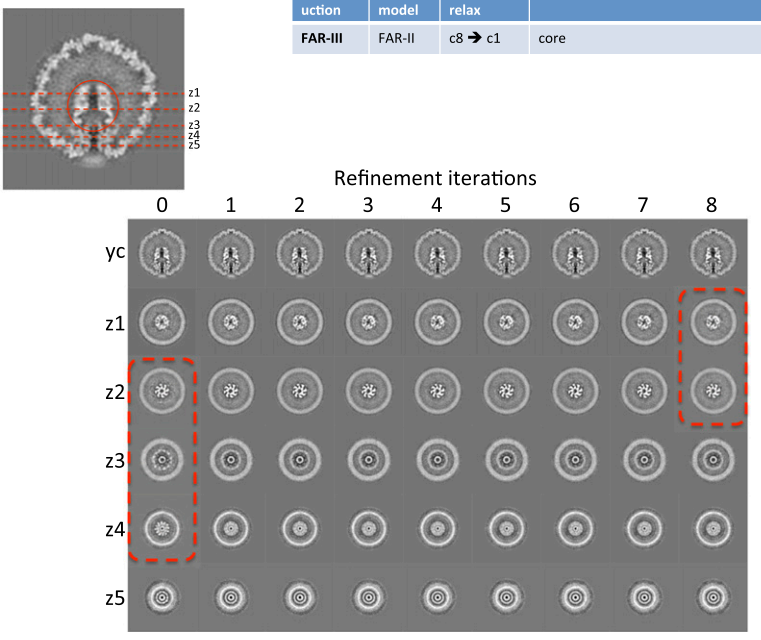

Fig. S7. Refinement convergence for focused asymmetric reconstruction III (FAR-III). Only the first eight iterations are shown. The numbers at the top (0–8) indicate the refinement iterations with 0 referring to the starting model (FAR-II). The first row (yc) shows the central section cut parallel to the portal/core stack axis. The subsequent rows (z1, z2, z3, z4, z5) show different sections cut perpendicular to the portal/core stack axis, as indicated in Fig. 1*C*. The red circle in the upper left corner indicates the region included in the alignment. The dashed red boxes indicate the sections with resolved features of the portal vertex.

Reconst ructions	Starting model	Symmetry relax	Region included in alignment
Icos	Random	N/A	entire capsid
SAR	Icos	icos → c1	entire capsid
FAR-IV	SAR	c8 → c1	core/portal
FAR-V	FAR-IV	c12 → c1	portal/shell
FAR-VI	SAR	c8 → c1	core

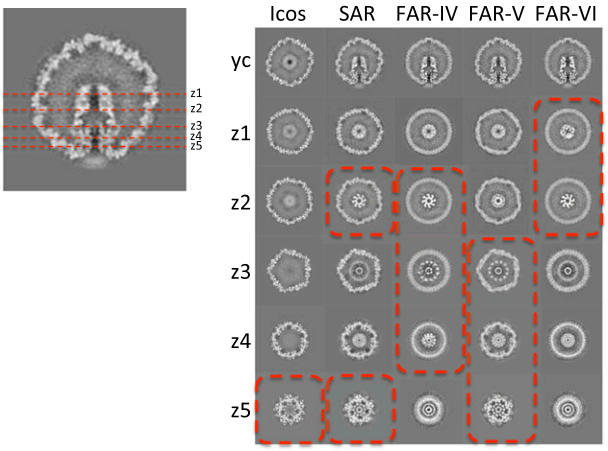

Fig. S8. Additional focused asymmetric reconstructions (FAR-IV, FAR-V, and FAR-VI). Each column represents one of the labeled reconstructions, Icos, SAR, FAR-IV, FAR-V, and FAR-VI, as indicated in the table above the sections. The reconstructions are also explained in the main text and in Table S1. Row 1 (yc) shows the central sections of the five reconstructions cut parallel to the portal/core stack axis. The subsequent rows (z1, z2, z3, z4, z5) show different sections cut perpendicular to the portal/core stack axis, as indicated in Fig. 1*C*. The dashed red boxes indicate the sections with resolved features of the portal vertex.

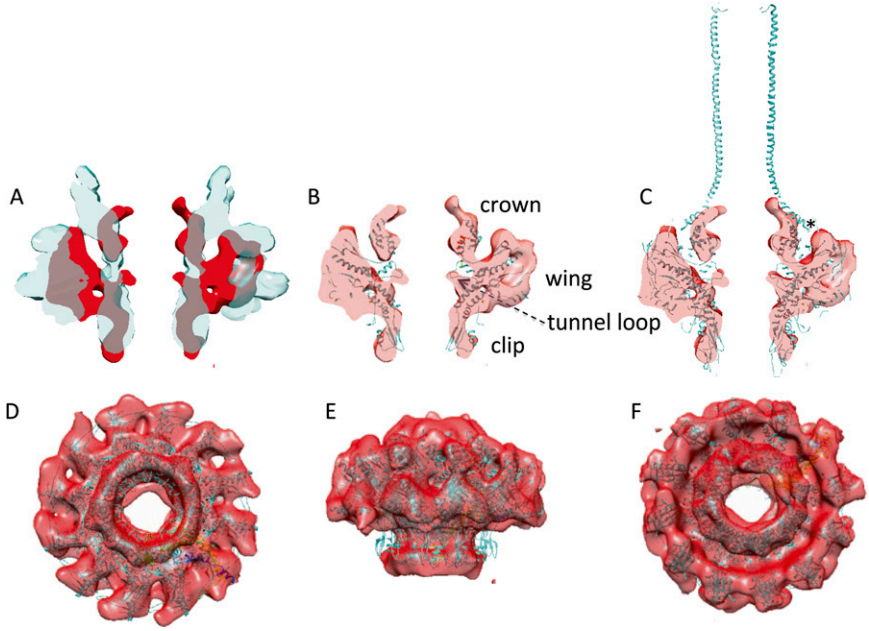

Fig. S9. Portal (gp8). (*A*) A 10-Å-thick central section of the T7 gp8 portal (segmented from a FAR-I reconstruction of capsid I; dark red) was superimposed on a cryo-EM structure of the isolated T7 portal (EMD-1231; light blue) (1). (*B* and *C*) X-ray crystal structure of bacteriophage SPP1 gp6 portal [Protein Data Bank (PDB) ID code 2JES] (2) (*B*) and P22 gp1 portal (PDB ID code 3LJ5) (3) (*C*) were superimposed on the same capsid I portal section (pink). (*D*–*F*) Surface views of the T7 capsid I portal structure (dark red) superimposed on the SPP1 model (light blue) viewed from clip (*D*), side (*E*), and crown (*F*), as indicated in *B*. The crystal structure of the SPP1 gp6 portal ring (UniProtKB ID P54309) was determined from a 13-fold, isolated ring (2). The SPP1 portal structure used in this figure is a 12-fold symmetry constrained fitting of the subunit of SPP1 gp6 13-fold ring to the T7 gp8 portal ring densities performed using UCSF Chimera command *fitmap*.

1. Agirrezabala X, et al. (2005) Structure of the connector of bacteriophage T7 at 8A resolution: Structural homologies of a basic component of a DNA translocating machinery. *J Mol Biol* 347(5):895–902.
2. Lebedev AA, et al. (2007) Structural framework for DNA translocation via the viral portal protein. *EMBO J* 26(7):1984–1994.
3. Olia AS, Prevelige PE, Jr., Johnson JE, Cingolani G (2011) Three-dimensional structure of a viral genome-delivery portal vertex. *Nat Struct Mol Biol* 18(5):597–603.

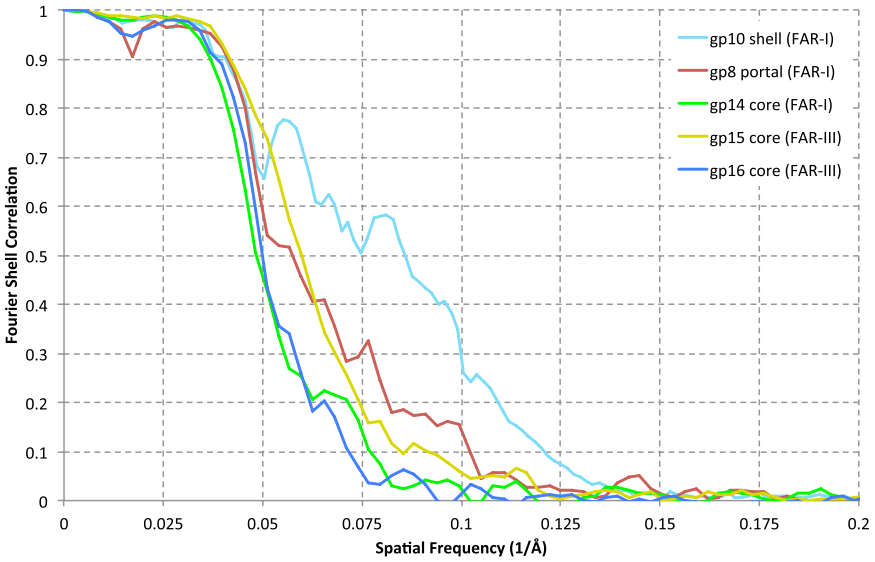

Fig. S10. Resolution evaluations. The structural components were segmented from the whole asymmetric reconstructions for the calculation of Fourier shell correlations. Using a 0.5 threshold criterion, the resolutions are determined to be 13, 17, 21, 17, and 20 Å for gp10 (icosahedral shell), gp8 (12-fold portal), gp14 (12-fold core stack layer), gp15 (8-fold core stack layer), and gp16 (4-fold core stack layer), respectively.

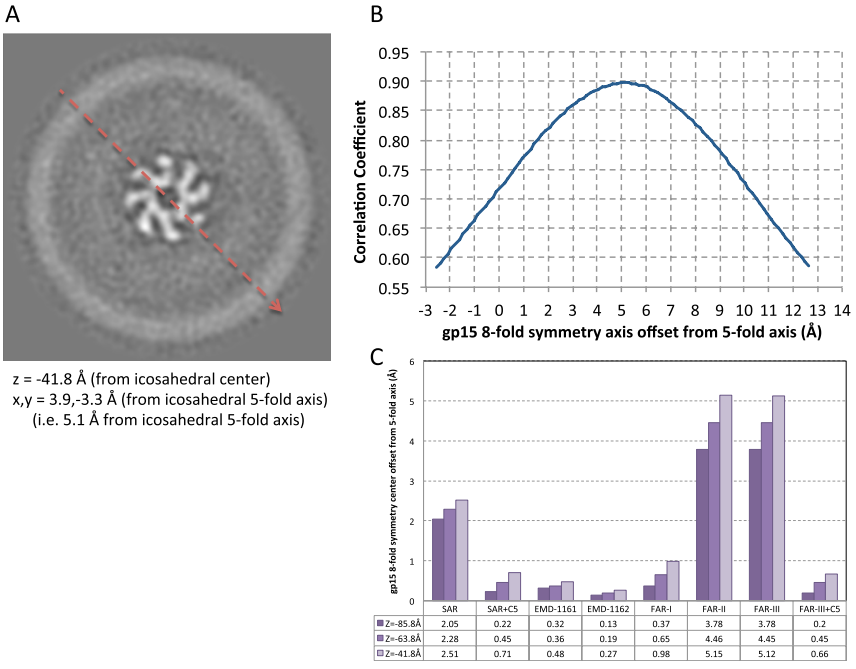

Fig. S11. Symmetry axis offset plot for the gp15 layer. (*A*) Section view of the eightfold gp15 core stack layer. (*B*) Plot of correlation coefficients representing the quality of eightfold symmetry for putative symmetry axis positions along the dashed line in *A*. (*C*) Comparison of gp15 symmetry axis center offsets for SAR, SAR+C5 (SAR reconstruction with additional fivefold symmetry imposed), EMD-1161 (T7 capsid I "asymmetric" reconstruction in ref. 1), EMD-1162 (T7 capsid I fivefold symmetric reconstruction in ref. 1), FAR-I, FAR-II, FAR-III, and FAR-III+C5 (FAR-III reconstruction with additional fivefold symmetry imposed). The offsets were determined by using the icosahedral fivefold axis as the reference and by maximizing the rotational symmetry quality for putative symmetry axis positions around the reference axis. The gp15 eightfold symmetry axis center in *A* was determined to be *x*, *y* = 3.9, −3.3 Å (i.e., 5.1 Å to the lower right direction along the arrow). This is the same eightfold symmetry axis offset shown in Fig. 4*A* (the right-most one of the triplet data points for gp15). In *B*, only the correlation coefficients along the line in *A* are shown. The peak in *B* is clearly located at 5.1 Å offset from 0 (i.e., the icosahedral fivefold axis position). Note that eightfold symmetry of gp15 was resolved only in SAR, FAR-II, and FAR-III, whereas the eightfold symmetry was either not resolved (EMD-1161, EMD-1162, and FAR-I) or intentionally smeared with fivefold averaging (SAR+C5, FAR-III+C5).

1. Agirrezabala X, et al. (2005) Maturation of phage T7 involves structural modification of both shell and inner core components. *EMBO J* 24(21):3820–3829.

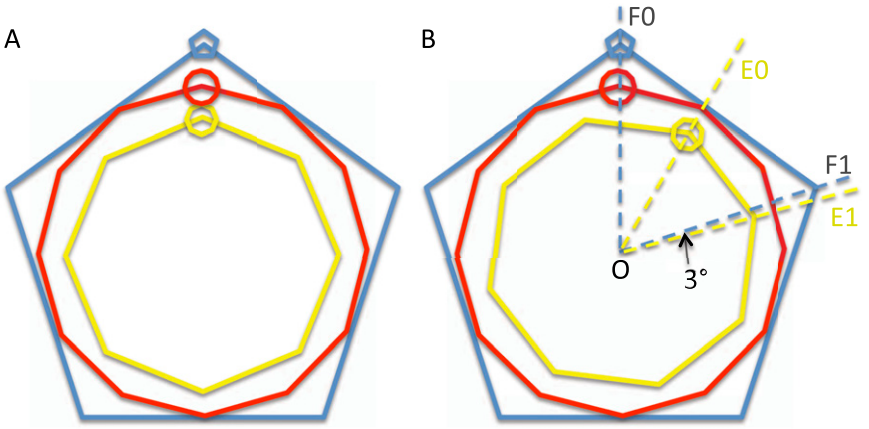

Fig. S12. Schematics for two different combinations of 5-, 12-, 8-fold symmetries. (*A*) The marked vertices of 5-, 12-, 8-fold rings are aligned. (*B*) The marked vertex in the 8-fold ring is now aligned to the right-side neighboring 12-fold vertex by rotating the 8-fold ring 30° to the right. In *B*, the best aligned fivefold vertex (F1) and eightfold vertex (E1) are offset by 3° (30° + 45° − 72° = 3°). Exhaustive enumeration of all possible combinations (Dataset S1) shows that one-third of all 5–12–8 combinations have 0 angular error as shown in *A*, and two-thirds of all combinations have 3° angular error as shown in *B* for the best-aligned 5-fold and 8-fold vertices.

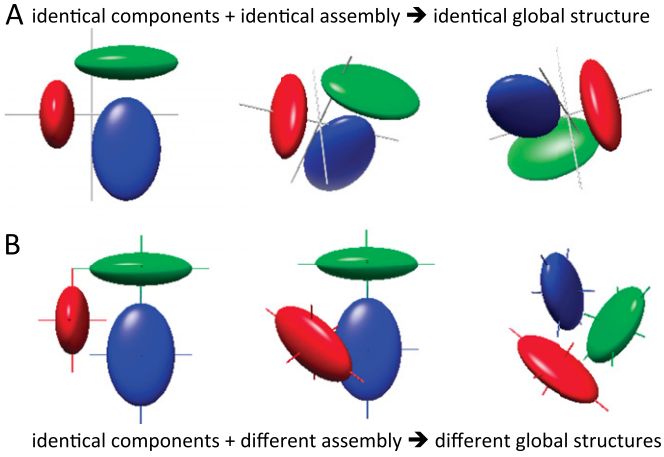

Fig. S13. Illustration of the concept of combinatorial assembly isomerism. (*A*) Identical global structure for three particles, for which the direction of view differs. Different copies (*Left*, *Center*, and *Right*) of the tripartite structure are superimposable and are only different in the direction of view and position. (*B*) Structures with combinatorial assembly isomerism. Particles are assembled from a common set of structural components, but are not superimposable, i.e., they have different global structures. Different copies (*Left*, *Center*, and *Right*) of the structure are different not only in their direction of view and position but also the relationships of the three (red, blue, green) components. The T7 capsid I structure belongs to this class (*B*) since the azimuthal angles of its five layers (gp10 shell, gp8 portal, gp14, gp15, and gp16 core stack layers) can vary independently among different particles.

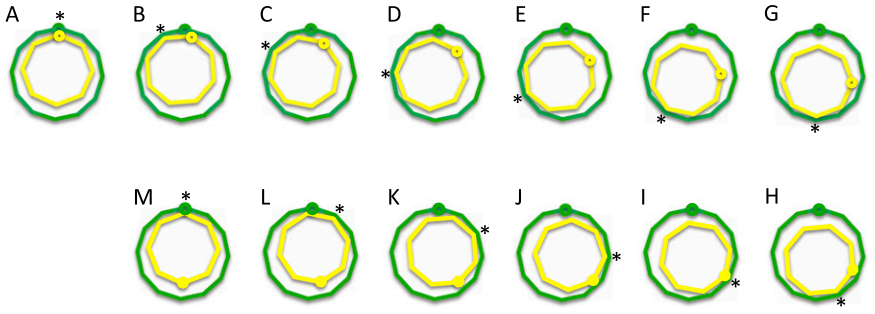

Fig. S14. The model for precession of the 8-fold gp15 layer around the 12-fold portal axis. In the starting state (*A*), the marked vertex of the slightly offset 8-fold gp15 ring is aligned to the marked vertex of the 12-fold portal/gp14 ring. Every 15° rotation of 8-fold ring (clockwise) aligns the next vertex of 8-fold core (separated by 45°) to the next vertex of 12-fold ring (30° + 15°=45°) (indicated by marker * in *B*). Twelve such rotations of the 8-fold ring will complete a revolution of precession (counterclockwise) (*A*→*M*) by returning the alignment of a vertex of the 8-fold ring to the same marked vertex of the 12-fold ring (*M*) as in the starting state (*A*). However, the eightfold ring has only rotated 180° (12*15° = 180°) around its own axis. The rate of 8-fold gp15 precession around the 12-fold portal axis is thus two times of the rate of its self-rotation in this model. This precession model is analogous to mechanical precession [http://en.wikipedia.org/wiki/Precession_(mechanical)].

Table S1. Three-dimensional reconstructions

Reconstructions	Starting model	Symmetry relax	Region included in alignment	Resolved features				
				gp10 (shell)	gp8 (portal)	gp14 (core)	gp15 (core)	gp16 (core)
Icos	Random	n/a	Entire capsid	✓				
SAR	Icos	Icos→c1	Entire capsid	✓			✓	
FAR-I	SAR	c5→c1	Shell/portal	✓	✓	✓		
FAR-II	FAR-I	c12→c1	Portal/core		✓	✓	✓	
FAR-III	FAR-II	c8→c1	Core				✓	✓
FAR-IV	SAR	c8→c1	Core/portal		✓	✓	✓	
FAR-V	FAR-IV	c12→c1	Portal/shell	✓	✓	✓		
FAR-VI	SAR	c8→c1	Core				✓	✓

Table S2. T7 phage capsid I proteins

Protein	UniProt ID	Length, aa	Mass, kDa	Role	Estimated copy number*	Found symmetry	Mass center offset, Å†
gp10A	P19726	345	37	Major shell protein	415	Icosahedral (T = 7)	0
gp8	P03728	536	59	Portal	12	C_{12}	1.0
gp14	P03724	196	21	Core	8–12	C_{12}	0.9
gp15	P03725	747	84	Core	8	C_8	4.5
gp16	P03726	1,318	144	Core	4	C_4	7.3

*From Serwer (1) and Cerritelli et al. (2). These estimates were based on phage state, and we assume that these five proteins have same copy number at capsid I state.
†Relative to the icosahedral fivefold axis passing the portal vertex.

1. Serwer P (1976) Internal proteins of bacteriophage T7. *J Mol Biol* 107(3):271–291.
2. Cerritelli ME, et al. (2003) A second symmetry mismatch at the portal vertex of bacteriophage T7: 8-fold symmetry in the procapsid core. *J Mol Biol* 327(1):1–6.

Other Supporting Information Files

Dataset S1 (PDF)